Title

Effector loss and gain drives pathogen host range at a fitness cost.

Authors

Marcus V. Merfa[1,2,3]**, Tracy E. Hawk[1,2], Jelmer W. Poelstra[4], Lillian Ebeling-Koning[1,2], Ervan Rodgers[1], Hannah Toth[1,2], Zachary Konkel[1,2], Jules Butchacas[1,2], Nathaniel Heiden[1,2†], Muhammad Uzair[3], Temitope F. Oladele[5], Godwin E. Oduokpaha[5], Rebecca D. Curland[6], Emmanuelle Lauber[7], Laurie Marsan[7], Zhaohui Liu[8], Ruth Dill-Macky[6], Laurent D. Noël[7], Horacio D. Lopez-Nicora[1], Jason C. Slot[1,2], Verónica Román-Reyna[1,2‡], Jonathan M. Jacobs[1,2]*

Affiliations

[1]Department of Plant Pathology, The Ohio State University; Columbus, 43210, USA.
[2]Infectious Disease Institute, The Ohio State University; Columbus, 43210, USA.
[3]Department of Microbiology, University of Tennessee, Knoxville; Knoxville, 37996, USA.
[4]Molecular and Cellular Imaging Center, The Ohio State University; Wooster, 44691, USA.
[5]The Bredesen Center for Interdisciplinary Research and Graduate Education, University of Tennessee, Knoxville; Knoxville, 37996, USA.
[6]Department of Plant Pathology, University of Minnesota; St. Paul, 55108, USA.
[7]LIPME, Université de Toulouse, INRAE, CNRS, Castanet-Tolosan, France.
[8]Department of Plant Pathology, North Dakota State University, Fargo, 58102, USA.
[†]Current address: Levo International, Inc.; Bloomfield, 06002, USA.
[‡]Current address: Department of Plant Pathology and Environmental Microbiology, The Pennsylvania State University; University Park, 16802, USA.
*Corresponding author. Email: jacobs.1080@osu.edu.
**Co-corresponding author. Email: mmerfaes@utk.edu.

Abstract

Epidemic preparedness depends on tracking microbial evolution that drives shifts in ecological behaviors such as disease emergence. However, the genetic constraints for microbial host adaptation to emerge for generalist and specialist behaviors remain poorly described. Here, we show that generalist cereal pathogen *Xanthomonas translucens* arose from a specialist ancestor via the loss of a single effector gene, *xopAL1*. Deleting barley-specialist *X. translucens xopAL1* recapitulated the host jump to wheat and demonstrates risk across each globally distributed genetic lineage. However, this niche expansion via XopAL1 loss incurs a significant pathogenic fitness cost to colonize barley. Moreover, the specialist lineage gained an additional effector gene, *xopAJ*, which enhanced virulence on barley while restricting oat infection, thereby reinforcing niche specialization. We further identified key host pathways mediating resistance to the specialist lineage of *X. translucens*, opening avenues for potentially identifying targets for crop improvement. Our work provides an experimentally validated evolutionary framework to understand mechanisms of intergenera host jump. Overall, we demonstrate that single events of gene loss and gain shape ecological behaviors of pathogens by creating a dynamic trade-off between niche breadth and specialization.

Keywords: pathogen evolution, niche specificity, host range, Type III secretion system, ecology.

Introduction

Disease outbreaks often result from pathogen evolution, leading to changes in microbial ecological behaviors such as niche specialization. Changes in niche-specificity may occur from single genetic loss or gain events[1,2] or the movement of genomic islands and plasmids that dictate the transitional behaviors such as niche shift between microbial pathogens and their hosts[3]. Niche alterations are universal and widespread in plant, human and animal epidemiology and have significant effect on host health outcomes[4]. Some pathogens have generalist behaviors with broad host ranges while others are highly specialized on a particular host or niche[5]. However, the underlying evolutionary and biological mechanisms often remain undefined for most niche changes, especially in plant agricultural systems.

Host range is a particular type of niche-specificity, and many pathogenic organisms can be found across the spectrum from generalist to specialist. The Gammaproteobacterial genus *Xanthomonas* limits agricultural production by causing diseases in over 400 identified plant species, although these pathogens as a whole infect close to 50 plant families. *Xanthomonas* bacteria in the generalist spectrum cause disease in a broad range of host genera with access to a breadth of potential hosts for resources, while specialists remain restricted to a particular species or genus (Fig. 1A and Fig. S1)[6-8]. Curiously, differences in niche-specificity of closely related plant pathogenic species and strains are often due to small changes in genome content[9-12] but the evolutionary mechanisms for niche specialization of *Xanthomonas* spp. remains poorly understood. Ultimately, understanding the spectrum and evolution of host range specificity will benefit prediction and mitigation of disease epidemics[5,13].

Bacterial organisms regularly secrete proteins and other molecules into the extracellular environment or directly into host cells to interact with their niche aiming at promoting growth, survival, colonization and virulence[14]. Many Gram-negative animal and plant bacterial pathogens, including *Xanthomonas spp.*, depend on a Type III secretion system (T3SS) for injecting effector proteins into the host cells to aid in pathogenesis[15,16]. Our previous work revealed that frequent loss and gain of a single gene encoding a Type II secreted cellulase effector, CbsA, promoted lifestyle switch for changes in tissue-specific host adaptation[2]. Here, we used a similar framework to define the evolution of host range shift in specialist and generalist subgroups (e.g. respectively, narrow and broad host range) of *Xanthomonas translucens*, arguably the most important re-emergent bacterial pathogen of cereals beyond rice[17-19]. We have determined that evolutionary loss and gain of Type III effectors (T3Es) govern the phenotypic switch between specialist and generalist behaviors of *X. translucens* subgroups for host range. Specifically, we determined that the broad host range lineage lost a single effector, XopAL1, to evade host defenses but at fitness cost on a primary host. Moreover, we assessed the potential for contemporary *X. translucens* specialist lineages to emerge via host jump, thus providing a framework for epidemiological tracking of particular lineages of risk.

Results

Xanthomonas translucens subgroups with differential host range behaviors encode significantly different T3E repertoires

Bacteria in the *X. translucens* species primarily infect grass and cereal plants in the Poaceae family, causing bacterial leaf streak (BLS) and blight, and black chaff of cereals[17,19]. Early documentation from the 1900s described the broad host range of generalist *X. translucens* pv.

undulosa (Xtu)[20,21]. This subgroup uses a wide range of metabolites upon infection of host plants[22] and causes disease in wheat, barley, rye, triticale, spelt, wild oat, ornamental asparagus, wild rice, and in a variety of wild grasses, totaling 12 plant genera (Fig. 1A and Fig. S1)[19-21,23-27]. In contrast, the closely related *X. translucens* pv. translucens (Xtt) is a specialist with limited metabolism that only causes disease in plants of the *Hordeum* genus (barley; Fig. 1A-B and Fig. S1)[20,22,24]. The main small grains affected by Xtt and Xtu are barley and wheat, respectively[17,24]. For example, upon spray inoculation for naturalistic entry and infection, Xtt and Xtu both caused water soaking symptom development in barley, but only generalist Xtu caused disease in wheat (Fig. 1B).

To better understand differences in niche specificity between the closely related (>97% average nucleotide identity)[28] but phylogenomically distinct Xtt and Xtu (Fig. 1A,C), comparative genomic analyses were conducted and revealed that over 3,000 core proteins are shared between them (Table S1). On the other hand, each subgroup had over 100 unique conserved proteins (Table S2). Secreted proteins, which are often associated with virulence[14], represented 3% and 3.5% of shared (core genome) and unique proteins (accessory genome), respectively (Tables S1-2). The number of unique, overall secreted proteins were not significantly different between Xtt and Xtu (Student's *t*-test; *P* value = 0.7772). However, specialist Xtt has a larger T3E repertoire than generalist Xtu (Wilcoxon rank-sum test; *P* value = 3.436 e-06).

Based on the biological importance of T3Es[15,16], we aimed to determine if there is a link between host range of *X. translucens* and encoded T3E repertoires. Hierarchical clustering of strains according to their encoded effector repertoires was congruent with the subspecies tree and with generalist and specialist behaviors (Fig. 1C). Specialist Xtt genomes encode an expanded effector repertoire that include XopAJ, XopAL1, XopE5, and HopW1 and an effector family expansion for XopP1 and XopP2. Only one unique T3E was identified in Xtu (XopE4), while seven were overall absent in this generalist subgroup (Fig. 1C). Moreover, Type III-secreted transcription activator-like (TAL) effectors were significantly more abundant in broad host range Xtu (Fig. S2; Student's *t*-test; *P* value = 0.02511). Highly virulent Xtu strains have previously been found to precisely manipulate plant hormone pathways via the Tal8 (synonym TalDC) effector to cause wheat bacterial leaf streak[29]. This effector is not encoded by low-virulence strains of Xtu or any Xtt strain (Fig. S2)[29]. We therefore hypothesize the TAL effector family expansion correlates with adaptation to new niches as these are highly evolvable repetitive elements[30]. While we only focused on non-TAL effectors in this study, future work will explore host adaptation based on this special and abundant class of effectors.

The T3E XopAL1 affects both host range and fitness in *X. translucens*

We hypothesized that individual T3Es might be responsible for host range differences between Xtt and Xtu. We first tested pathogenicity on both barley and wheat for Δ*hrcT* mutants that lack a critical component for the *X. translucens* T3SS by inoculating leaves via syringe infiltration[16]. Δ*hrcT* mutants of Xtt and Xtu did not cause symptoms in barley or wheat (Fig. S3A). Unlike the lack of symptom development upon natural infection via spray (Fig. 1B), Xtt caused chlorosis in wheat when inoculated via syringe infiltration (Fig. S3A). This has been described as a non-host or non-pathogenic response unlike the well-described hypersensitive response and is an undefined plant response that prevents disease development by Xtt[8,16,31-33].

139 We then aimed to define if a unique Xtt effector prevented wheat pathogenesis by screening for
140 loss of chlorosis. Individual deletions of the four Xtt-unique or single Xtu-unique effector genes
141 did not alter pathogenicity in barley or chlorosis development in wheat upon infiltration
142 inoculation except for *xopAL1* (Fig. S3). Notably, *xopAL1* deletion in Xtt produced water
143 soaking symptom development in wheat similar to Xtu BLS (Fig. S3A). Moreover,
144 complementation of the Xtt Δ*xopAL1* mutant strain or *xopAL1* introduction into the true wheat
145 pathogen Xtu (Xtu miniTn7::*xopAL1*) triggered development of the non-pathogenic, chlorosis
146 phenotype in wheat (Fig. S3). Introduction of the other three Xtt-unique effectors in Xtu did not
147 trigger the wheat chlorotic response (Fig. S3B).
148
149 These findings were further assessed by spray inoculation, an infection method more similar to
150 natural infections than syringe infiltration. Xtt Δ*xopAL1* caused BLS similar to Xtu on wheat and
151 barley (Fig. 2A). On the other hand, introduction of this effector into Xtu disrupted its ability to
152 cause disease in wheat (Fig. 2A). Curiously, deletion of *xopAL1* significantly decreased the
153 symptomatic leaf area of barley inoculated via spray (Fig. 2B). Because of the reduced virulence
154 of Xtt Δ*xopAL1* and Xtu although pathogenic is infrequently isolated from barley[34], we suspected
155 that XopAL1 plays a role in bacterial fitness beyond restricting the ability of Xtt to cause disease
156 in wheat. Significantly higher endophytic populations of Xtt wild-type (WT) and Xtu
157 miniTn7::*xopAL1* were observed in barley leaves in comparison to non-*xopAL1*-encoding strains
158 (Xtt Δ*xopAL1* and Xtu WT; Fig. 2C). Moreover, Xtt Δ*xopAL1* had a similar population to Xtu in
159 wheat upon syringe infiltration, whereas introduction of this effector in Xtu significantly reduced
160 its population to similar levels as Xtt WT (Fig. S4). Altogether, these results demonstrated that
161 *xopAL1* is a fitness factor for Xtt virulence and colonization in specialized host barley, but which
162 restricts its ability to cause disease in wheat in an effector-dependent manner possibly via
163 XopAL1 recognition.
164
165 A cereal genotype diversity panel containing known susceptible hosts to Xtu was screened to
166 assess if other plant species display a similar *xopAL1*-dependent resistance mechanism (Table
167 S3). All screened hexaploid wheat genotypes (*Triticum aestivum* L., BBAADD genotype)
168 presented a *xopAL1*-dependent resistance response against Xtt. Diploid (einkorn, AA genotype)
169 and tetraploid (durum and emmer, BBAA genotypes) wheat genotypes were overall more
170 susceptible to Xtt in a XopAL1-independent manner. Curiously, all tested Triticale lines
171 (hexaploid genotype BBAARR) displayed a *xopAL1*-dependent resistance response against Xtt.
172 Despite Triticale being a wheat-rye hybrid[35], no *xopAL1*-dependent resistance was observed in
173 rye, which remained resistant to Xtt. Curiously, genomic introduction of *xopAL1* into Xtu did not
174 convert this subgroup into a non-pathogen of Triticale, as opposed to wheat. We therefore
175 hypothesize that wheat resistance against Xtt may be mostly encoded by the DD sub-genome,
176 which has the annual grass *Aegilops tauschii* Coss. as the donor species[36].
177
178 A subset of this cereal genotype diversity panel was screened with individual mutant strains for
179 the other Xtt-unique effectors (*xopAJ*, *xopE5*, and *hopW1*; Table S4). Our analysis revealed a
180 *xopAJ*-dependent resistance response of oat (*Avena sativa* L., AACCDD genotype) against Xtt
181 (Table S4; Fig. S5). Results thus suggest that this Xtt-unique effector determines its host range
182 for causing disease in oat. Nevertheless, the downstream analyses described here focused mainly
183 on XopAL1 due to its role in determining the ability of *X. translucens* to cause disease in its two
184 main economic host plants, wheat and barley[17,24].

185
186 ***xopAL1* has been lost in Xtu and presents an inherent risk for host jump by Xtt**
187 Plant pathogen populations may shift and diversify their encoded virulence factor repertoires to
188 avoid recognition by the host immune system[1,37]. We therefore tested if the emergence of broad
189 host range Xtu correlated with the loss of *xopAL1*. Xtu was suggested to have diverged from a
190 Xtt ancestor[38], and we examined *xopAL1* evolution with maximum likelihood phylogenetic
191 comparisons of whole genomes and the *xopAL1* locus neighborhood (Fig. 3A-B; Figs. S6-7), and
192 by reconciling with the *xopAL1* tree (Fig. S8A). Specific neighborhoods of *xopAL1* were defined
193 across the *X. translucens* species (Fig. 3A and Fig. S9). Our phylogenetic hypothesis testing of
194 the *X. translucens xopAL1* locus determined that this effector was lost in Xtu (neighborhood type
195 1) during its divergence from a common ancestor with Xtt (neighborhood type 2; Fig. 3B-C).
196 Loss of *xopAL1* was common across other *X. translucens* lineages. Three other inferred losses of
197 *xopAL1* with acquisition of different genes replacing this effector were observed in subgroups
198 with neighborhood type 4 (Fig. 3B). The origin of *xopAL1* (neighborhood type 2) was
199 parsimoniously inferred in *X. translucens* to occur after divergence from a common ancestor
200 with pathovar cerealis and strain ICMP 16317 in pathovar pistaciae (Xtp; neighborhood type 5;
201 Fig. 3B). In addition, there was truncation of *xopAL1* in pathovar graminis (Xtg) by direct
202 transposon insertion 5' of the remaining sequence fragment (neighborhood type 3; Fig. 3B and
203 Fig. S8B). For comparison, we analyzed the evolution of *xopE5* and *hopW1* (other Xtt-unique
204 effector genes) and also observed loss in Xtu for both (Figs. S10-11, respectively).
205
206 Risk assessment is key for epidemic preparedness, but there is often a lack of precise knowledge
207 about what genetic events lead to emergence, and about the potential of organisms to change
208 their niche. Because loss of *xopAL1* allowed Xtu to jump host to wheat, we examined if deletion
209 of this effector gene could lead to host jump for the three described, globally-distributed Xtt
210 genomic subgroups (K0, K1, and K2)[34,39]. The deletion of *xopAL1* in representative K0, K1 and
211 K2 strains led to host expansion to wheat (Fig. 3D). Xtt lineages are globally important in barley
212 production systems[39], and all have an inherent pathogenic capacity in wheat production systems
213 based on *xopAL1* loss.
214
215 ***xopAJ* has been gained by Xtt and enhances virulence in barley**
216 Gene gain is another mechanism for niche shift in *Xanthomonas*[2]. Using the same framework as
217 for *xopAL1*, we determined that the oat-limiting effector gene *xopAJ* was originated in Xtt
218 (neighborhood 2) after divergence with Xtu (neighborhood 1; Figs. S12-13). This gene was also
219 gained in related pistachio-infecting *X. translucens* (Xtp) strain CFBP 8304 but further truncated
220 via transposon insertion (neighborhood 3; Figs. S12-13). *xopAJ* is not encoded by any other *X.*
221 *translucens* subgroup and is not encoded by Xtt in the same locus as other *xopAJ*-encoding
222 *Xanthomonas* spp. (Fig. S14). Moreover, Xtt-encoded *xopAJ* is more phylogenetically closely
223 related to *xopAJ* encoded by a distant species, *Paracidovorax citrulli*, than to *xopAJ* encoded by
224 other *Xanthomonas* spp. (Fig. S15). These results suggest that *xopAJ* evolution is dynamic and
225 was gained in Xtt by horizontal gene transfer but lost by dicot pathogen Xtp. We hypothesized
226 that gain of *xopAJ* by Xtt increases its adaptive fitness to colonize barley. Deletion of *xopAJ* in
227 Xtt significantly decreased the symptomatic leaf area of barley upon spray inoculation (Fig.
228 S16A-B), but no significant changes were observed for endophytic populations of the pathogen
229 (Fig. S16C). Altogether, results show that gain of *xopAJ* enhanced virulence of Xtt in barley,
230 while not affecting fitness for plant colonization.

XopAL1 mediates global transcriptional reprogramming in wheat leading to a chlorotic non-host response

The basis of chlorosis development in a non-host response is widespread in *Xanthomonas*-plant interactions but remains unclear[8,31,32]. For instance, a distant XopAL1 ortholog encoded by *Xanthomonas campestris* pv. campestris (Fig. S8) also triggered chlorosis development in wheat when transformed in Xtu (Fig. S17). We thus carried out RNA sequencing (RNA-seq) to elucidate the mechanistic basis of non-host response that restricts bacterial infection. Expression profiles were compared between wheat leaves inoculated with *xopAL1*-encoding strains (Xtt WT and Xtu miniTn7::*xopAL1*), non-encoding strains (Xtt Δ*xopAL1* and Xtu WT), and mock-inoculated leaves. A principal component analysis (PCA) of the RNA-seq count data demonstrated that samples clustered in two primary transcriptional profiles in a *xopAL1*-dependent manner, reflecting the ability of strains to cause disease in wheat or not (Fig. 4A). Accordingly, much higher numbers of significantly differentially expressed genes (DEGs) were identified in plants inoculated with Xtt and Xtu encoding *xopAL1* when compared to mock-treated samples (12,397 and 9,118 DEGs, respectively; Table S5) and in comparison to non-encoding strains of these subgroups (607 and 285 DEGS, respectively; Table S5) (Fig. 4B).

A gene ontology (GO) term enrichment analysis was performed to investigate the specific plant processes in wheat that led to the non-host response. Our analysis revealed that upregulated DEGs in response to inoculation with Xtt and Xtu expressing *xopAL1* were significantly enriched in GO terms associated with immunity, induced defense response, defense signaling, and programmed cell death (Fig. 4C; Table S5). On the other hand, significant overrepresentation of GO terms associated with photosynthetic pathways, including chloroplast and chlorophyll processes, were observed among the downregulated DEGs in response to strains expressing *xopAL1* (Fig. 4C; Table S5). Based on this, we hypothesized that chlorosis is the result of reduced photosynthetic activity and chlorophyll content in wheat upon XopAL1 recognition. Indeed, we observed significantly lower chlorophyll concentration in wheat leaves inoculated with *xopAL1*-encoding Xtt and Xtu in comparison to those inoculated with non-encoding strains and mock-inoculated leaves (Fig. 4D). These findings indicate that recognition of XopAL1 in wheat results in extensive transcriptional changes that ultimately lead to a non-host type of resistance response.

Discussion

Emerging infectious diseases often result from microbial niche shift. Multiple genetic mechanisms control emergence including gene loss and gain. Genome and episome reduction are strongly associated with host specialization and gain can promote adaptation to a particular environment or resist control interventions (e.g. antibiotics)[40,41]. Here, were have determined that loss and gain of single T3Es control specialist and generalist behaviors of Xtt and Xtu for host range. Specifically, our results collectively demonstrate that a) XopAL1 is both a fitness and virulence requirement for Xtt; b) this effector is a determinant of host range since its loss contributed for host expansion of Xtu to wheat by circumventing an otherwise effector-triggered defense response of this host plant; and c) gain of XopAJ by Xtt limited its ability to cause disease in oat but contributes for full virulence in barley.

Bacterial pathogens commonly colonize host plants by delivering secreted factors that alter plant cellular processes to promote virulence, but these same factors can also trigger plant immune responses that restrict infection if recognized by cognate plant resistance (R) proteins[15,16]. Absence or presence of specific T3Es dictates host range of plant pathogens in an effector-triggered immunity (ETI) -dependent manner. Examples of effectors affecting host range include the XopAG, XopQ, and AvrBsT effectors of *Xanthomonas* spp.[9,10,12,32], and HopQ1-1 effector of *Pseudomonas syringae*[11]. Moreover, effectors have demonstrated fitness requirements for leaf colonization in particular hosts[37,42]. For instance, absence of AvrBsT expands the host range of *Xanthomonas perforans* while decreasing the fitness of this pathogen in tomato fields[42].

These studies demonstrate how T3E repertoires may vary in response to resistance within individual cropping or model plant systems but lack an evolutionary framework. Here, we determined the phylogenetically-supported evolutionary history and ecological function of T3E loss and gain events related to fitness and host range. Using the generalist model Xtu, we posit that *xopAL1* was one of multiple loss events that led to emergence of this pathogenic generalist subgroup. Xtu has lost other niche-specific factors for tissue-specificity. Our previous work demonstrated that loss of the vascular-associated pathogen gene *cbsA* is frequently associated with non-vascular tissue colonization. This gene is encoded by the vascular, specialist Xtt but was lost in non-vascular, generalist Xtu via transposon insertion[2]. Here, we have also observed truncation of *xopAL1* in Xtg, and *xopAJ* in Xtp via transposon insertion. Transposons shape microbial niche-specificity, and these insertion sequence (IS) elements are major drivers of evolutionary ecological shifts of bacterial and fungal species[2,43-45]. Overall, we hypothesize that gene loss, frequently mediated by IS elements, is a common strategy for niche shifts across behaviors.

Interestingly, XopAJ, which we have determined here as a host range-limiting factor for *X. translucens* in oat, was gained in Xtt and contributes for virulence in barley. We speculate that gain of effectors upon host specialization provides resource access on a preferred host. XopAJ (synonym of AvrRxo1) was initially described as a host range-limiting factor of the rice pathogen *X. oryzae* pv. oryzicola (Xoc) when inoculated into maize lines carrying the cognate resistance gene Rxo1[46]. This effector has been shown to suppress pattern-triggered immunity (PTI) responses of host and non-host plants[47], and to enhance virulence of Xoc[48]. Xtt is limited to barley (*Hordeum* spp.), and it remains to be determined whether XopAJ displays similar molecular functional roles for host colonization and pathogen virulence as observed in other *Xanthomonas* spp.

Hosts respond dramatically different to specialized and generalist pathogens and could be used to inform resistance trait discovery. Components of the wheat defense response pathway identified here via RNA-seq compose a valuable pool of candidates to identify the interactor(s) of XopAL1 and generate resistance in other hosts including barley. Moreover, we observed downregulation of chloroplast processes, which play a central role in plant immunity[49]. Together, our RNA-seq results help to understand the basis of the chlorotic non-host response that includes upregulation of defense responses with downregulation of photosynthetic processes.

Preparedness for mitigation of new epidemics, especially when host jump occurs, depends on strong knowledge of the evolution of niche shift. The research described here provides a

322 framework for reconstructing the evolutionary history of host jump in an important cereal
323 pathogen and allows us to predict pathogen emergence based on gene loss and gain. Based on
324 our results, we developed a tested evolutionary model for *X. translucens* intergenera host jump
325 centered on effector gene loss and gain (Fig. 5). Xtu is a generalist that has fewer T3Es, and loss
326 of *xopAL1* promoted its broad host range behavior. Conversely, gain of *xopAJ* in the specialist
327 Xtt restricted its ability to cause disease in oat. A practical implication of our model is that
328 management of BLS of wheat and oat must include surveillance of all lineages of Xtt in addition
329 to Xtu due to their inherent risk for jumping hosts based on loss of single genes. Ultimately, this
330 work demonstrated that the shift between specialist and generalist subgroups of *X. translucens*
331 for host range is modulated by presence and absence of single genes, with gene loss and gain
332 being major drivers for changing niches and ecological behaviors of pathogens.
333
334 **Materials and Methods**
335
336 **Bacterial strains, plasmids, and culture conditions**
337 Bacterial strains and plasmids used in this study are listed in Table S6. *Xanthomonas* strains were
338 recovered from -80ºC glycerol stocks and grown for two days at 28ºC on nutrient agar (NA) or
339 nutrient broth (NB) (3 g/L beef extract, 5 g/L peptone, 15 g/L agar). When needed, the
340 antibiotics kanamycin (Km), gentamicin (Gm), or cycloheximide (CHX) were used at
341 concentrations of 50 µg/ml, 5 µg/ml, and 50 µg/ml, respectively. Sterile deionized water was
342 used for suspending cells in liquid. *Escherichia coli* strains were cultured in Luria-Bertani (LB)
343 medium at 37ºC. LB was supplemented with kanamycin (50 µg/ml), gentamicin (10 µg/ml), or
344 ampicillin (100 µg/ml) whenever necessary. *E. coli* WM3064, a diaminopimelic acid (DAP)
345 auxotrophic strain used for conjugation transformation, was grown as described above, but with
346 LB medium supplemented with DAP (200 µM).
347
348 **Recombinant DNA techniques**
349 Genomic DNA of respective strains was isolated using the Monarch Genomic DNA Purification
350 kit (New England Biolabs). Polymerase chain reactions (PCR) were performed using Q5 High-
351 Fidelity DNA Polymerase (New England Biolabs) for cloning sequences into plasmid vectors of
352 interest or using Quick-Load *Taq* 2X Master Mix (New England Biolabs) for other processes.
353 PCR reactions were carried out using standard manufacturer protocols in a ProFlex PCR System
354 thermal cycler (Applied Biosystems). PCR products and agarose gel fragments were purified
355 using the QIAquick PCR and Gel Cleanup kit (QIAGEN). Competent cells of *E. coli* strains
356 were made and transformed using the Mix & Go! *E. coli* Transformation Buffer set (Zymo
357 Research). Plasmid DNA was isolated from overnight cultures of *E. coli* using the QIAprep Spin
358 Miniprep kit (QIAGEN).
359
360 Transformation of Xtt UPB820 and Xtu UPB513 with respective plasmids (Table S6) was
361 performed by electroporation (1.8 kV, 200 Ω, 25 µF and a time constant lower than 5 ms). Some
362 Xtt UPB820 strains were transformed via electroporation with pPneo-GFP for kanamycin
363 resistance and GFP expression (Table S6). Transformation of Xtt UPB787 and XtKm7 was made
364 via conjugation using the *E. coli* donor strain WM3064. In summary, Xtt strains were grown
365 overnight in 40 mL of NB (28 ºC, 220 rpm), and *E. coli* WM3064 strains were grown overnight
366 in 20 mL of LB + DAP + respective antibiotic (37 ºC, 220 rpm). After, Xtt and *E. coli* cells were
367 collected by centrifugation (4,000 rpm for 10 minutes), suspended into the same volume of

368 media (40 mL of NB for Xtt and 20 mL of LB + DAP for *E. coli* WM3064), centrifuged again
369 and suspended with adequate volume of media to obtain an optical density at 600nm (OD_{600}) of
370 3.0. Then, Xtt and *E. coli* cells were combined at a 1:1 ratio and 200 µL aliquots were spotted on
371 top of MF-Millipore MCE membranes (25 mm diameter, 0.45 µm pore size; Merck Millipore
372 Ltd.) overlaid on NA + DAP. Eight membranes were spotted per transformation event. Plates
373 were incubated for 24 hours at 28ºC, and membranes were then recovered by using sterile
374 forceps and placed into conical tubes containing 20 mL of NB. Cells were removed from
375 membranes by vortexing on maximum for 1 minute, and membranes were removed using sterile
376 forceps. At last, cells were collected by centrifugation (4,000 rpm for 10 minutes), suspended in
377 1 mL of NB, diluted by 10-fold serial dilution until 10^{-2} and 500 µL aliquots of the 10^{-1} and 10^{-2}
378 suspensions were then plated on NA + antibiotic selective medium (150 mm diameter plates) for
379 growth of transformed cells.
380
381 Clean deletion of genes of interest (GOI) in strains of *X. translucens* (Table S7) was made via
382 *sacB* counter-selection using the pK18mobsacB plasmid, as previously described[2]. Clean
383 deletion of each GOI was confirmed via PCR (Table S8). Complementation of *xopAL1* and
384 *xopAJ* in the respective mutant strains of each in Xtt UPB820 was also performed via the
385 pK18mobsacB plasmid. The upstream and downstream regions of each gene, together with their
386 open reading frames, were amplified altogether using the upstream region forward primer and
387 the downstream region reverse primer (Table S8) and then cloned into pK18mobsacB at the
388 HindIII restriction site via Gibson Assembly (New England Biolabs). Insertion of *xopAL1* and
389 *xopAJ* back into their original loci was confirmed via PCR (Table S8).
390
391 To obtain the constructs for genomic insertion via miniTn*7*, the open reading frames of each GOI
392 containing promoter and terminator regions were amplified by PCR and then fused (when
393 needed) and cloned into pUC18miniTn*7*T-Gm at the HindIII restriction site via Gibson
394 Assembly (New England Biolabs). The obtained constructs were confirmed via PCR (Table S8)
395 and transformed into Xtu UPB513 together with pTNS3 (Table S6) to promote transposition and
396 single gene insertion. Transformant cells were selected by plating on NA + Gm and confirmed
397 for GOI genomic insertion by PCR (Table S8).
398
399 The $xopAL1_{Xcc8004}$ gene (400-bp promoter plus 100-bp terminator, amplicons LM169-170 and
400 LM171-LM172; Table S8) was cloned from *X. campestris* pv. campestris (Xcc) strain 8004 by
401 GoldenGate strategy using *Bsa*I-mediated restriction-ligation into pEL667, a GoldenGate-
402 compatible derivative of pBBR1MCS2. Ligation products were introduced into *E. coli* by
403 electroporation and conjugated into Xcc using pRK2073 as a helper plasmid in triparental
404 matings.
405
406 **Plant growth conditions and inoculation methods**
407 Barley (*Hordeum vulgare* L. cv. Morex) and wheat (*Triticum aestivum* L. varieties 'Chinese
408 Spring', RB07, Glenn, and AGS2055) seeds were germinated and grown in growth chambers
409 with cycles of 16 hours of light per day at 22º to 24 ºC and 70% relative humidity for leaf syringe
410 infiltration inoculations, or in greenhouse conditions for temperature, relative humidity and light
411 for spray inoculation. In both experiments, seeds were germinated directly in potting mix (PRO-
412 MIX BX General Purpose; Premier Tech Growers and Consumers Inc.) in 3.5 inches diameter
413 square pots (four seeds per pot; Kord Products).

For spray inoculation, the primary leaf (counting from the bottom) of seven-day-old wheat and barley plants was sprayed till run off on the abaxial and adaxial surfaces with water-based bacterial inocula (OD_{600} of 0.5) or sterile deionized water as mock control. After leaves were dry, pots with plants were transferred to trays filled with approximately 0.5 inch of tap water. Trays were then covered for four days to promote high relative humidity, which facilitates infection via spray inoculation. Plants were kept for two additional days in greenhouse conditions after removing the covers and development of water soaking symptoms was evaluated at six days post inoculation. Individual inoculated leaves were taped to transparency film sheets and pictures were taken using a LED light box (Tikteck). When appropriate, the total and symptomatic leaf areas were measured via the ImageJ software[50] by using a set scale. A standardized length of 5 cm from the top to bottom of each inoculated leaf was used for individual measurements. The percentage of symptomatic leaf area was then calculated using the obtained areas. The experiment was conducted independently twice, with 23 to 24 independent plants being inoculated for each treatment in each independent replicate.

For bacterial population quantification in barley following spray inoculation, leaves inoculated as described above were collected at six days post inoculation. The leaves were surface-disinfested by soaking into 70% ethanol for five seconds, followed by two consecutive rinses in sterile deionized water for five seconds each. This was done so that the isolation targeted those bacterial cells that naturally moved and multiplied into the inner leaf tissue. After, two leaf discs were collected at each side of the main leaf vein using a standardized length of 2.5 cm from the top to bottom of each inoculated leaf by using a 2.5 mm diameter punch (Acuderm Inc.). Leaf discs were then flash frozen in liquid nitrogen and stored at -80ºC until processed. For bacterial isolation, leaf discs were ground in 100 µL of sterile deionized water in 2-mL microcentrifuge tubes containing a sterile 5 mm diameter stainless steel bead (QIAGEN) using the TissueLyzer II apparatus (30 Hz for 1 minute; QIAGEN). Samples were then transferred to 96-well plates (Thermos Scientific), diluted by 10-fold serial dilutions and plated as 5 µL drops in triplicates in selective media (NA + CHX + Km for Xtt strains transformed with pPneo-GFP, and NA + CHX + Gm for Xtu strains with miniTn*7* genomic insertion). Colony forming units (CFU) were enumerated after three days of incubation at 28 ºC. The experiment was conducted independently twice, with 23 to 24 independent plants being inoculated for each treatment in each independent replicate.

For infiltration inoculation, the first two leaves (counting from the bottom) of fourteen-day-old plants (wheat and barley) were inoculated using needleless syringes. Bacterial strains were suspended in sterile deionized water (OD_{600} of 0.1) for inoculation. Control plants (mock) were inoculated with sterile deionized water. Three to four independent plants were inoculated for each treatment, and experiments were conducted independently at least twice. Development of symptoms was recorded three days post inoculation (dpi), in which lesions associated with pathogenicity were recorded (water soaking – disease development; chlorosis – non-host response; no symptom – no pathogenicity). Pictures of inoculated leaves were taken at 3 dpi by placing them on top of a black non-reflective photography display board (Neewer) and using the camera of a cell phone mounted on a tripod (UBeesize) with a LED cell phone circle light (QIAYA). Germination, growth, inoculation, and evaluation of the plant species used to screen a

459 cereal genotype diversity panel (Tables S3-4) with Xtt and Xtu strains were performed as
460 described for infiltration inoculation.
461
462 Inoculations for bacterial growth curves performed in planta were made via leaf syringe
463 infiltration, as described above, but using a lower optical density of each bacterial suspension
464 (OD_{600} of 0.001). Plants were inoculated in triplicates per time point and treatment, and samples
465 were collected at 2, 24, 72, 120, and 168 hours post inoculation using a 2.5 mm diameter punch
466 (Acuderm Inc.), flash frozen in liquid nitrogen and stored at -80 ºC until processed. Bacterial
467 isolation, serial dilution, plating, and enumeration were performed as described above.
468 Experiments were performed independently twice.
469
470 **Whole genome sequencing**
471 Genomic DNA for Xtt strains Colorado, CIX84, UPB545, UPB787, and UPB820, and Xtu strain
472 UPB513, was extracted using Genomic-tip 20/G and the Genomic DNA Buffer Set (QIAGEN)
473 and then sequenced as previously described[51]. Briefly, PacBio long-read, single-molecule real-
474 time sequencing was used to sequence extracted genomic DNAs, and assembly was performed
475 via Flye v2.4[52] for strains CIX84 and UPB545, and via HGAP v4 (PacBio) for strains Colorado,
476 UPB787, UPB820, and UPB513 using default settings. Whole genomes were deposited at
477 GenBank under accession numbers CP159781 for Xtt UPB545, CP159782 for Xtt CIX84, and
478 JBEFAI000000000 for Xtu UPB513 (Table S9). Availability of the genomes of Xtt strains
479 Colorado, UPB787, and UPB820 is shown in Table S9.
480
481 **Pangenome analyses to identify core and unique proteins among Xtt and Xtu**
482 Pangenome analysis to identify core and unique proteins encoded by all analyzed Xtt and Xtu
483 strains (Tables S1-2 and Table S9) was performed by comparing the gene presence/absence
484 output matrix obtained when analyzing genomes via Panaroo v1.3.3, a tool designed to perform
485 core and pangenome comparisons of prokaryotes[53]. Core proteins are determined here as proteins
486 encoded by all strains in both pathovars translucens and undulosa. On the other hand, unique
487 proteins of a specific pathovar are determined here as proteins encoded by all strains of a specific
488 pathovar but are not encoded by any strain of the other pathovar. The proteome of a
489 representative strain of each pathovar was searched for secretion signals using SignalP v6.0 to
490 predict secreted proteins[54]. Proteomes were obtained by annotating genomes via Prokka v1.14.6
491 (see below)[55]. SignalP results were then used to identify which core and unique proteins of Xtt
492 and Xtu are predicted to be secreted. Proteins in which a secretion signal was identified but were
493 predicted to locate to the outer membrane or periplasm were excluded when calculating the
494 percentage of secreted proteins within core and unique proteins. Additional genes encoded
495 uniquely by subsets of strains belonging to one pathovar or the other were also identified and
496 analyzed as described above to compare percentages of uniquely secreted proteins in each
497 pathovar via statistical analysis (described below). Hypothetical proteins were not considered to
498 calculate the proportion of secreted proteins in the core genome but were considered when
499 performing this analysis in genes found uniquely in pathovars translucens or undulosa. We
500 manually curated secretion of proteins annotated as hypothetical by searching for encoded
501 functions using the blastp algorithm (<https://blast.ncbi.nlm.nih.gov/Blast.cgi?PAGE=Proteins>)
502 and retrieving the best hit for each searched protein.
503
504 **Phylogenomic and phylogenetic analyses**

Phylogenomic trees depicting the evolutionary relationships of examined *Xanthomonas* species for host range comparisons (Fig. 1A and Fig. S1) were constructed from well-supported 1780 single-copy orthologous genes (SCOs) trees. SCOs were determined via OrthoFinder[56], and individual SCO phylogenies were constructed by first aligning via *mafft* v7.487[57], trimming via *ClipKIT* v1.3.0[58], and building the phylogeny via *IQ-TREE* v2.2.6 with 1,000 ultrafast bootstrap iterations[59]. Individual SCO trees with at least 75% average node support were concatenated for a multigene phylogenomic tree by applying best predicted evolutionary models to each SCO partition.

All other whole-genome phylogenies were performed based on core genome alignment. Genomes of interest were annotated via Prokka v1.14.6 specifying the appropriate genus and species with the "--genus" and "--species" options, respectively, and otherwise with default settings[55], followed by core genome alignment using Panaroo v1.3.3 with a core threshold of 0.98 and option "—clean-mode strict"[53]. Alignments were then filtered for recombination by first using maximum likelihood recombination inference through ClonalFrameML v1.12[60] followed by alignment masking with maskrc-svg v0.5 (https://github.com/kwongj/maskrc-svg), and trees were built using IQ-TREE v2.2.2.7 with 5,000 ultrafast bootstrap replicates.

A phylogenetic tree for the *xopAL1* locus neighborhood, which includes four upstream and five downstream genes of *xopAL1*, was constructed by first running Parsnp v1.7.4[61] to align the nucleotide sequence of this neighborhood from the reference strain Xtt UPB820 (extracted with the GetFasta command from the BEDTools suite)[62] with the full genomes of the other selected assemblies (Table S9), then converting the Parsnp output to a FASTA alignment using Harvesttools v1.2[61], and finally inferring a tree with IQ-TREE v2.2.2.7 using 5,000 ultrafast bootstrap replicates. The same method was used to generate phylogenetic trees of the *xopE5* (six upstream and five downstream genes) and *hopW1* (five upstream and seven downstream genes) loci neighborhoods. An amino acid sequence-based phylogenetic tree of the *xopAJ* locus neighborhood (six upstream and four downstream genes of *xopAJ*) was generated by identifying orthologs of each of these genes in the genomes of interest via OrthoFinder v2.5.5, aligning them individually with MAFFT v7.520 using default parameters. Poorly aligned regions were removed from alignments using Trimal v1.5.0 using the '-automated1' method[63]. A concatenated locus tree was inferred using IQ-TREE v2.2.2.7 with 1,000 ultrafast bootstrap replicates and gene concordance factors were calculated for each node.

Phylogenetic trees for individual genes within the *xopAL1* locus neighborhood were constructed by first identifying orthologs to these genes in Xtt UPB820 via OrthoFinder v2.5.5, extracting the focal sequences with BEDTools GetFasta, aligning them with MAFFT v7.520, and inferring trees using IQ-TREE v2.2.2.7 with 1,000 ultrafast bootstrap replicates. *xopAL1* encoded by the outgroup representative *Ralstonia solanacearum* strain 10314 was included for the phylogenetic tree of *xopAL1*. The phylogenetic trees of *xopE5*, *hopW1*, and *xopAJ* were constructed via the same method but using *Paraburkholderia nemoris* strain RL18-011-BIC-A and *Ralstonia mannitolilytica* strain LMG 18090 as outgroups for *xopE5*, *Pseudomonas amygdali* strain CFBP 1650 and *Erwinia psidii* strain LPF 534 as outgroups for *hopW1*, and *Paracidovorax citrulli* strains AAC00-1 and DSM 17060 as outgroups for *xopAJ*.

550 Classification of strains of *X. translucens* pv. translucens in the K0, K1, and K2 sub-genomic
551 groups, as determined by life identification numbers (LINs) calculated with LINbase, was
552 performed as previously described[39].
553
554 **Identification of Type III secretion system effector repertoires**
555 The effector repertoires of strains of *X. translucens* were identified as previously described via
556 BLAST 2.8.1+ blastx algorithm[39], excluding transcription activator-like effectors (TALEs).
557 Briefly, a database of known *Xanthomonas* spp. Type III secretion system effectors
558 (https://euroxanth.ipn.pt/doku.php?id=bacteria:t3e:effectors) was used as subject to search the
559 query genomes. Results were filtered for hits with coverage of over 200 amino acids and percent
560 amino acid identity of at least 60%. TALEs were identified and classified using AnnoTALE
561 v1.5[64]. The effector repertoire heat map and the Type III effector cluster dendrogram
562 (hierarchical clustering) figures were generated using the ComplexHeatmap[65] and RColorBrewer
563 (https://cran.r-project.org/web/packages/RColorBrewer/index.html) packages in R v4.1.0[66].
564
565 **RNA-sequencing and analysis**
566 To determine wheat response to XopAL1, an RNA-seq analysis was performed. Wheat plants
567 were grown as described above and inoculated with Xtt UPB820 WT, Xtu UPB513 WT, Xtt
568 UPB820 Δ*xopAL1,* Xtu UPB513 miniTn*7*::*xopAL1,* or a water (mock) control. Each treatment
569 had three independent replicates, and bacterial inoculations were performed at an OD_{600} of 0.001.
570 Tissue was collected 24 hours post inoculation, flash frozen in liquid nitrogen, and homogenized
571 using a sterile 5 mm diameter stainless steel bead (QIAGEN) using the TissueLyzer II apparatus
572 (30 Hz for 1 minute; QIAGEN). Total RNA was extracted using TRIzol (Thermo Scientific) and
573 DNA was removed using the TURBO DNA-free kit (Thermo Scientific) following
574 manufacturer's guidelines. Plant and 16S ribosomal depletion was performed and total RNA
575 libraries were constructed using random oligos. RNA libraries were multiplexed and sequenced
576 using a NextSeq 2000 (Illumina) with 150-bp paired-end reads and a target of 30 million reads
577 per sample.
578
579 RNA-seq analysis was performed using the Nextflow/nf-core "rnaseq" pipeline v3.10.1[67], using
580 the *Triticum aestivum* L. cv. 'Chinese Spring' reference genome (version 2.1) obtained from
581 Phytozome. RNA-seq data were processed using the nf-core RNA-seq pipeline implemented
582 with Nextflow. This pipeline included adapter trimming with TrimGalore! v0.6.5
583 (<https://www.bioinformatics.babraham.ac.uk/projects/trim_galore/>), alignment of reads to the
584 wheat genome with STAR v2.7.10b[68], and transcript abundance estimation with Salmon
585 v1.10.1[69]. Quality metrics for each step were aggregated using MultiQC v1.14[70]. The read count
586 Table output by the pipeline was used to identify differentially expressed genes using the
587 DESeq2 package[71]. Genes with an adjusted *P* value (FDR) < 0.05 were considered significantly
588 differentially expressed. Genes with a $\log_2$ fold change ($\log_2$FC) > 0 were defined as upregulated,
589 while those with $\log_2$FC < 0 were classified as downregulated. The raw RNA-seq fastq files are
590 available at GenBank under accession number GSE299780.
591
592 Normalized gene counts produced from DESeq2 were used to generate a principal component
593 analysis (PCA) plot using ggplot2 in R[72]. Gene ontology (GO) analysis was performed to
594 identify enriched biological functions among differentially expressed genes. GO term
595 annotations for each gene in the wheat 'Chinese Spring' reference genome were obtained from

596 Phytozome (<https://phytozome-next.jgi.doe.gov>). Enrichment analysis was conducted
597 separately for upregulated and downregulated genes using the Gene Ontology Resource
598 (<http://geneontology.org>)[73-75]. Only significantly overrepresented GO terms (adjusted *P* value
599 < 0.05) were considered enriched among downregulated or upregulated genes. Selected GO
600 terms related to plant defense and photosynthesis were visualized using a Cleveland dot plot
601 generated in R with ggplot2.
602
603 **Chlorophyll concentration measurement in wheat leaves**
604 Xtt and Xtu strains were suspended in sterile deionized water (OD_{600} of 0.1) and inoculated into
605 fourteen-day-old wheat leaves (*Triticum aestivum* L. genotype 'Chinese Spring'; second leaf
606 counting from the bottom) using needless syringes as described above for infiltration inoculation.
607 Control plants (mock) were inoculated with sterile deionized water. At three days post
608 inoculation, leaves were collected and the chlorophyll concentration in inoculated areas was
609 measured in triplicates in each leaf using the MC-100 Chlorophyll Concentration Meter (Apogee
610 Instruments, Inc.). Chlorophyll concentration was measured as micromoles per square meter
611 ($\mu mol\ m^{-2}$) of leaf using the manufacturer's specific settings for wheat and the standard
612 operational protocol for the instrument. The experiment was conducted independently twice,
613 with six to nine independent plants being inoculated for each treatment in each independent
614 replicate.
615
616 **Identification and visualization of genomic neighborhoods**
617 To identify the *xopAL1*, *xopAJ*, *xopE5*, and *hopW1* genomic neighborhoods in *Xanthomonas*
618 spp., Prokka-annotated genomes were aligned and visualized via progressiveMauve using default
619 settings[76] to determine flanking genes and neighborhoods. Genomes were then uploaded to the
620 Benchling cloud-based platform (https://www.benchling.com) to extract the sequences of
621 genomic neighborhoods in GBK format, which were submitted to cluster comparison analysis
622 via Clinker v0.0.23 (default settings) to generate figures[77].
623
624 **Protein alignment and visualization**
625 Amino acid sequence alignment of representative sequences of XopAL1 within *Xanthomonas*
626 spp. was performed via the T-Coffee Multiple Sequence Alignment Server[78] and visualized using
627 pyBoxShade (https://github.com/mdbaron42/pyBoxshade). Percent coverage and similarity were
628 determined via the blastp algorithm.
629
630 **Data analysis and visualization**
631 Data from number of proteins encoded by Xtt and Xtu strains (total and unique proteins), and
632 data from number of TAL effectors encoded by both of these subgroups were compared by two-
633 tailed Student's *t*-test. Data from number of proteins in the effector repertoires of both subgroups
634 (excluding TAL effectors), from bacterial growth in barley leaves inoculated via spray at six
635 days post inoculation, and from chlorophyll concentration in wheat leaves inoculated via
636 infiltration at three days post inoculation were analyzed by Kruskal-Wallis test followed by
637 Wilcoxon rank-sum test in R v4.1.0. Data from bacterial growth curves in planta upon syringe
638 infiltration were analyzed per time point by one way analysis of variance (ANOVA) followed by
639 Tukey's post-hoc test in the log-transformed data. Assumptions were tested on the residuals of
640 the model, and the normality of the data was assessed by the Shapiro-Wilk test in R v4.1.0 under
641 the package rstatix (https://rpkgs.datanovia.com/rstatix/). Data from bacterial growth in barley

642 leaves inoculated via spray at four days post inoculation were analyzed via ANOVA followed by
643 Tukey's post-hoc test upon checking normality of the data. The original data (x) of the
644 percentage of secreted proteins uniquely found in pathovars translucens or undulosa, and of the
645 percentage of symptomatic leaf area in barley leaves inoculated via spray were submitted to a
646 transformation that combines the arcsine and square root functions ($y = \arcsin(\sqrt{x}/100)$). The
647 normality of data was then assessed by the Shapiro-Wilk test, and treatments were analyzed
648 using the two-tailed Student's *t*-test. Phylogenetic trees were visualized, and mid-point rooted via
649 FigTree v1.4.4. (http://tree.bio.ed.ac.uk/). Genomic neighborhoods were visualized using
650 Clinker.
651
652 **References**

653 1 Inoue, Y. *et al.* Evolution of the wheat blast fungus through functional losses in a host
654 specificity determinant. *Science* **357**, 80–83 (2017).
655 https://doi.org/doi:10.1126/science.aam9654
656 2 Gluck-Thaler, E. *et al.* Repeated gain and loss of a single gene modulates the evolution of
657 vascular plant pathogen lifestyles. *Sci Adv* **6**, eabc4516 (2020).
658 3 Melnyk, R. A., Hossain, S. S. & Haney, C. H. Convergent gain and loss of genomic
659 islands drive lifestyle changes in plant-associated Pseudomonas. *The ISME Journal* **13**,
660 1575–1588 (2019). https://doi.org/10.1038/s41396-019-0372-5
661 4 Baker, R. E. *et al.* Infectious disease in an era of global change. *Nat Rev Microbiol* **20**,
662 193–205 (2022). https://doi.org/10.1038/s41579-021-00639-z
663 5 Barrett, L. G., Kniskern, J. M., Bodenhausen, N., Zhang, W. & Bergelson, J. Continua of
664 specificity and virulence in plant host-pathogen interactions: causes and consequences.
665 *New Phytol* **183**, 513–529 (2009). https://doi.org/10.1111/j.1469-8137.2009.02927.x
666 6 Jacques, M. A. *et al.* Using ecology, physiology, and genomics to understand host
667 specificity in Xanthomonas. *Annu Rev Phytopathol* **54**, 163–187 (2016).
668 https://doi.org/10.1146/annurev-phyto-080615-100147
669 7 Jacobs, J. M., Pesce, C., Lefeuvre, P. & Koebnik, R. Comparative genomics of a cannabis
670 pathogen reveals insight into the evolution of pathogenicity in Xanthomonas. *Front Plant*
671 *Sci* **6**, 431 (2015). https://doi.org/10.3389/fpls.2015.00431
672 8 Dubrow, Z. E. *et al.* Cruciferous weed isolates of Xanthomonas campestris yield insight
673 into pathovar genomic relationships and genetic determinants of host and tissue
674 specificity. *Mol Plant Microbe Interact* **35**, 791–802 (2022).
675 https://doi.org/10.1094/mpmi-01-22-0024-r
676 9 Escalon, A. *et al.* Variations in type III effector repertoires, pathological phenotypes and
677 host range of Xanthomonas citri pv. citri pathotypes. *Mol Plant Pathol* **14**, 483–496
678 (2013). https://doi.org/10.1111/mpp.12019
679 10 Gochez, A. M. *et al.* A functional XopAG homologue in Xanthomonas fuscans pv.
680 aurantifolii strain C limits host range. *Plant Pathology* **64**, 1207–1214 (2015).
681 https://doi.org/10.1111/ppa.12361
682 11 Ferrante, P. *et al.* Contributions of the effector gene hopQ1-1 to differences in host range
683 between Pseudomonas syringae pv. phaseolicola and P. syringae pv. tabaci. *Mol Plant*
684 *Pathol* **10**, 837–842 (2009). https://doi.org/10.1111/j.1364-3703.2009.00577.x
685 12 Schwartz, A. R. *et al.* Phylogenomics of Xanthomonas field strains infecting pepper and
686 tomato reveals diversity in effector repertoires and identifies determinants of host
687 specificity. *Front Microbiol* **6**, 535 (2015). https://doi.org/10.3389/fmicb.2015.00535

13 Morris, C. E. & Moury, B. Revisiting the concept of host range of plant pathogens. *Annu Rev Phytopathol* **57**, 63–90 (2019). https://doi.org/10.1146/annurev-phyto-082718-100034

14 Alvarez-Martinez, C. E. *et al.* Secrete or perish: The role of secretion systems in Xanthomonas biology. *Comput Struct Biotechnol J* **19**, 279–302 (2021). https://doi.org/10.1016/j.csbj.2020.12.020

15 Timilsina, S. *et al.* Xanthomonas diversity, virulence and plant-pathogen interactions. *Nat Rev Microbiol* **18**, 415–427 (2020). https://doi.org/10.1038/s41579-020-0361-8

16 Pesce, C. *et al.* Comparative genomics identifies a novel conserved protein, HpaT, in proteobacterial type III secretion systems that do not possess the putative translocon protein HrpF. *Front Microbiol* **8**, 1177 (2017). https://doi.org/10.3389/fmicb.2017.01177

17 Sapkota, S., Mergoum, M. & Liu, Z. The translucens group of Xanthomonas translucens: Complicated and important pathogens causing bacterial leaf streak on cereals. *Mol Plant Pathol* **21**, 291–302 (2020). https://doi.org/10.1111/mpp.12909

18 Friskop, A. *et al.* Increase of bacterial leaf streak in hard red spring wheat in North Dakota and yield loss considerations. *Phytopathology* **113**, 2103–2109 (2022).

19 Ledman, K. E., Curland, R. D., Ishimaru, C. A. & Dill-Macky, R. Xanthomonas translucens pv. undulosa identified on common weedy grasses in naturally infected wheat fields in Minnesota. *Phytopathology* **111**, 1114–1121 (2021). https://doi.org/10.1094/phyto-08-20-0337-r

20 Jones, L. R., Johnson, A. G. & Reddy, C. S. Bacterial blights of barley and certain other cereals. *Science* **44**, 432–433 (1916).

21 Smith, E. F., Jones, L. R. & Reddy, C. S. The black chaff of wheat. *Science* **50**, 48 (1919).

22 Roman-Reyna, V. *et al.* The timing of bacterial mesophyll infection shapes the leaf chemical landscape. *Microbiol Spectr* **12**, e0413823 (2024). https://doi.org/10.1128/spectrum.04138-23

23 Bragard, C., Verdier, V. & Maraite, H. Genetic diversity among Xanthomonas campestris strains pathogenic for small grains. *Applied and Environmental Microbiology* **61**, 1020–1026 (1995).

24 Bragard, C. *et al.* Xanthomonas translucens from small grains: diversity and phytopathological relevance. *Phytopathology* **87**, 1111–1117 (1997).

25 Curland, R. D., Saad, Y. S., Ledman, K. E., Ishimaru, C. A. & Dill-Macky, R. First report of bacterial leaf streak caused by Xanthomonas translucens pv. undulosa on intermediate wheatgrass (Thinopyrum intermedium) in Minnesota. *Plant Dis* **104**, 279 (2020).

26 Curland, R. D., Hallada, K. R., Ledman, K. E. & Dill-Macky, R. First report of bacterial leaf streak caused by Xanthomonas translucens pv. undulosa on cultivated wild rice (Zizania palustris) in Minnesota. *Plant Dis* **105**, 2711 (2021). https://doi.org/10.1094/pdis-02-21-0407-pdn

27 Rademaker, J. L. *et al.* Classification and identification of Xanthomonas translucens isolates, including those pathogenic to ornamental asparagus. *Phytopathology* **96**, 876–884 (2006). https://doi.org/10.1094/phyto-96-0876

28 Goettelmann, F. *et al.* Complete genome assemblies of all Xanthomonas translucens pathotype strains reveal three genetically distinct clades. *Front Microbiol* **12**, 817815 (2021). https://doi.org/10.3389/fmicb.2021.817815

29 Peng, Z. *et al.* Xanthomonas translucens commandeers the host rate-limiting step in ABA biosynthesis for disease susceptibility. *Proc Natl Acad Sci U S A* **116**, 20938–20946 (2019). https://doi.org/10.1073/pnas.1911660116

30 Erkes, A., Reschke, M., Boch, J. & Grau, J. Evolution of Transcription Activator-Like Effectors in Xanthomonas oryzae. *Genome Biol Evol* **9**, 1599–1615 (2017). https://doi.org/10.1093/gbe/evx108

31 Curland, R. D., Gao, L., Hirsch, C. D. & Ishimaru, C. A. Localized genetic and phenotypic diversity of Xanthomonas translucens associated with bacterial leaf streak on wheat and barley in Minnesota. *Phytopathology* **110**, 257–266 (2020). https://doi.org/10.1094/phyto-04-19-0134-r

32 Adlung, N. *et al.* Non-host Resistance Induced by the Xanthomonas Effector XopQ Is Widespread within the Genus Nicotiana and Functionally Depends on EDS1. *Front Plant Sci* **7**, 1796 (2016). https://doi.org/10.3389/fpls.2016.01796

33 Balint-Kurti, P. The plant hypersensitive response: concepts, control and consequences. *Mol Plant Pathol* **20**, 1163–1178 (2019). https://doi.org/10.1111/mpp.12821

34 Curland, R. D. *et al.* Genetic diversity and virulence of wheat and barley strains of Xanthomonas translucens from the upper midwestern United States. *Phytopathology* **108**, 443–453 (2018). https://doi.org/10.1094/phyto-08-17-0271-r

35 Stace, C. A. Triticale: a case of nomenclatural mistreatment. *Taxon* **36**, 445–452 (1987).

36 Levy, A. A. & Feldman, M. Evolution and origin of bread wheat. *Plant Cell* **34**, 2549–2567 (2022). https://doi.org/10.1093/plcell/koac130

37 Vera Cruz, C. M. *et al.* Predicting durability of a disease resistance gene based on an assessment of the fitness loss and epidemiological consequences of avirulence gene mutation. *Proc Natl Acad Sci U S A* **97**, 13500–13505 (2000). https://doi.org/10.1073/pnas.250271997

38 Clavijo, F. *et al.* Complete genome sequence resource for Xanthomonas translucens pv. undulosa MAI5034, a wheat pathogen from Uruguay. *Phytopathology* **112**, 2036–2039 (2022). https://doi.org/10.1094/phyto-01-22-0025-a

39 Heiden, N., Roman-Reyna, V., Curland, R. D., Dill-Macky, R. & Jacobs, J. M. Comparative genomics of barley-infecting Xanthomonas translucens shows overall genetic similarity but globally distributed virulence factor diversity. *Phytopathology* **113**, 2056–2061 (2023). https://doi.org/10.1094/phyto-04-22-0113-sc

40 McCutcheon, J. P. & Moran, N. A. Extreme genome reduction in symbiotic bacteria. *Nat Rev Microbiol* **10**, 13–26 (2011). https://doi.org/10.1038/nrmicro2670

41 Roman-Reyna, V. *et al.* Live tracking of a plant pathogen outbreak reveals rapid and successive, multidecade plasmid reduction. *mSystems* **9**, e0079523 (2024). https://doi.org/10.1128/msystems.00795-23

42 Abrahamian, P. *et al.* The type III effector AvrBsT enhances Xanthomonas perforans fitness in field-grown tomato. *Phytopathology* **108**, 1355–1362 (2018). https://doi.org/10.1094/phyto-02-18-0052-r

43 Oggenfuss, U. *et al.* A population-level invasion by transposable elements triggers genome expansion in a fungal pathogen. *Elife* **10** (2021). https://doi.org/10.7554/eLife.69249

44 Krishnan, P. *et al.* Transposable element insertions shape gene regulation and melanin production in a fungal pathogen of wheat. *BMC Biol* **16**, 78 (2018). https://doi.org/10.1186/s12915-018-0543-2

45 Ferreira, R. M. *et al.* A TALE of transposition: Tn3-like transposons play a major role in the spread of pathogenicity determinants of Xanthomonas citri and other xanthomonads. *mBio* **6**, e02505–02514 (2015). https://doi.org/10.1128/mBio.02505-14

46 Zhao, B. *et al.* The avrRxo1 gene from the rice pathogen Xanthomonas oryzae pv. oryzicola confers a nonhost defense reaction on maize with resistance gene Rxo1. *Mol Plant Microbe Interact* **17**, 771–779 (2004). https://doi.org/10.1094/mpmi.2004.17.7.771

47 Popov, G., Fraiture, M., Brunner, F. & Sessa, G. Multiple Xanthomonas euvesicatoria Type III Effectors Inhibit flg22-Triggered Immunity. *Mol Plant Microbe Interact* **29**, 651–660 (2016). https://doi.org/10.1094/mpmi-07-16-0137-r

48 Liu, H. *et al.* The bacterial effector AvrRxo1 inhibits vitamin B6 biosynthesis to promote infection in rice. *Plant Commun* **3**, 100324 (2022). https://doi.org/10.1016/j.xplc.2022.100324

49 Littlejohn, G. R., Breen, S., Smirnoff, N. & Grant, M. Chloroplast immunity illuminated. *New Phytol* **229**, 3088–3107 (2021). https://doi.org/10.1111/nph.17076

50 Schneider, C. A., Rasband, W. S. & Eliceiri, K. W. NIH Image to ImageJ: 25 years of image analysis. *Nat Methods* **9**, 671–675 (2012).

51 Roman-Reyna, V. *et al.* Genome resource of barley bacterial blight and leaf streak pathogen Xanthomonas translucens pv. translucens strain UPB886. *Plant Dis* **104**, 13–15 (2020). https://doi.org/10.1094/pdis-05-19-1103-a

52 Kolmogorov, M., Yuan, J., Lin, Y. & Pevzner, P. A. Assembly of long, error-prone reads using repeat graphs. *Nature Biotechnology* **37**, 540–546 (2019). https://doi.org/10.1038/s41587-019-0072-8

53 Tonkin-Hill, G. *et al.* Producing polished prokaryotic pangenomes with the Panaroo pipeline. *Genome Biol* **21**, 180 (2020). https://doi.org/10.1186/s13059-020-02090-4

54 Teufel, F. *et al.* SignalP 6.0 predicts all five types of signal peptides using protein language models. *Nat Biotechnol* **40**, 1023–1025 (2022). https://doi.org/10.1038/s41587-021-01156-3

55 Seemann, T. Prokka: rapid prokaryotic genome annotation. *Bioinformatics* **30**, 2068–2069 (2014). https://doi.org/10.1093/bioinformatics/btu153

56 Emms, D. M. & Kelly, S. OrthoFinder: phylogenetic orthology inference for comparative genomics. *Genome Biol* **20**, 238 (2019). https://doi.org/10.1186/s13059-019-1832-y

57 Katoh, K., Misawa, K., Kuma, K. & Miyata, T. MAFFT: a novel method for rapid multiple sequence alignment based on fast Fourier transform. *Nucleic Acids Res* **30**, 3059–3066 (2002).

58 Steenwyk, J. L., Buida, T. J., 3rd, Li, Y., Shen, X. X. & Rokas, A. ClipKIT: A multiple sequence alignment trimming software for accurate phylogenomic inference. *PLoS Biol* **18**, e3001007 (2020). https://doi.org/10.1371/journal.pbio.3001007

59 Minh, B. Q. *et al.* IQ-TREE 2: New models and efficient methods for phylogenetic inference in the genomic era. *Mol Biol Evol* **37**, 1530–1534 (2020). https://doi.org/10.1093/molbev/msaa015

60 Didelot, X. & Wilson, D. J. ClonalFrameML: efficient inference of recombination in whole bacterial genomes. *PLoS Comput Biol* **11**, e1004041 (2015). https://doi.org/10.1371/journal.pcbi.1004041

61 Treangen, T. J., Ondov, B. D., Koren, S. & Phillippy, A. M. The Harvest suite for rapid core-genome alignment and visualization of thousands of intraspecific microbial genomes. *Genome Biology* **15**, 524 (2014).

62 Quinlan, A. R. & Hall, I. M. BEDTools: a flexible suite of utilities for comparing genomic features. *Bioinformatics* **26**, 841–842 (2010). https://doi.org/10.1093/bioinformatics/btq033

63 Capella-Gutierrez, S., Silla-Martinez, J. M. & Gabaldon, T. trimAl: a tool for automated alignment trimming in large-scale phylogenetic analyses. *Bioinformatics* **25**, 1972–1973 (2009). https://doi.org/10.1093/bioinformatics/btp348

64 Grau, J. *et al.* AnnoTALE: bioinformatics tools for identification, annotation, and nomenclature of TALEs from Xanthomonas genomic sequences. *Sci Rep* **6**, 21077 (2016). https://doi.org/10.1038/srep21077

65 Gu, Z., Eils, R. & Schlesner, M. Complex heatmaps reveal patterns and correlations in multidimensional genomic data. *Bioinformatics* **32**, 2847–2849 (2016). https://doi.org/10.1093/bioinformatics/btw313

66 Ihaka, R. & Gentleman, R. R: A language for data analysis and graphics. *J. Comput. Graph. Stat.* **5**, 299–314 (1996).

67 Ewels, P. A. *et al.* in *Nat Biotechnol* Vol. 38 276–278 (2020).

68 Dobin, A. *et al.* STAR: ultrafast universal RNA-seq aligner. *Bioinformatics* **29**, 15–21 (2013). https://doi.org/10.1093/bioinformatics/bts635

69 Patro, R., Duggal, G., Love, M. I., Irizarry, R. A. & Kingsford, C. Salmon provides fast and bias-aware quantification of transcript expression. *Nat Methods* **14**, 417–419 (2017). https://doi.org/10.1038/nmeth.4197

70 Ewels, P., Magnusson, M., Lundin, S. & Käller, M. MultiQC: summarize analysis results for multiple tools and samples in a single report. *Bioinformatics* **32**, 3047–3048 (2016). https://doi.org/10.1093/bioinformatics/btw354

71 Love, M. I., Huber, W. & Anders, S. Moderated estimation of fold change and dispersion for RNA-seq data with DESeq2. *Genome Biol* **15**, 550 (2014). https://doi.org/10.1186/s13059-014-0550-8

72 Wickham, H. *ggplot2: Elegant Graphics for Data Analysis*. (Springer-Verlag New York, 2016).

73 Carbon, S. *et al.* AmiGO: online access to ontology and annotation data. *Bioinformatics* **25**, 288–289 (2009). https://doi.org/10.1093/bioinformatics/btn615

74 Thomas, P. D. *et al.* Gene Ontology Causal Activity Modeling (GO-CAM) moves beyond GO annotations to structured descriptions of biological functions and systems. *Nat Genet* **51**, 1429–1433 (2019). https://doi.org/10.1038/s41588-019-0500-1

75 Thomas, P. D. *et al.* PANTHER: Making genome-scale phylogenetics accessible to all. *Protein Sci* **31**, 8–22 (2022). https://doi.org/10.1002/pro.4218

76 Darling, A. E., Mau, B. & Perna, N. T. progressiveMauve: multiple genome alignment with gene gain, loss and rearrangement. *PLoS One* **5**, e11147 (2010). https://doi.org/10.1371/journal.pone.0011147

77 Gilchrist, C. L. M. & Chooi, Y.-H. clinker & clustermap.js: automatic generation of gene cluster comparison figures. *Bioinformatics* **37**, 2473–2475 (2021). https://doi.org/10.1093/bioinformatics/btab007

78 Di Tommaso, P. *et al.* T-Coffee: a web server for the multiple sequence alignment of protein and RNA sequences using structural information and homology extension. *Nucleic Acids Res* **39**, W13–17 (2011). https://doi.org/10.1093/nar/gkr245

Acknowledgments

We thank Carine Gris (LIPME, Université de Toulouse, INRAE, CNRS) for the help in providing the *X. campestris* pv. campestris strains. We acknowledge funding from the Agriculture and Food Research Initiative SCRI grant no. 2020-51181-32154, from the INRAE SPE project XANTHOHS to E.L., L.M. and L.D.N., and from the American Malting Barley Association. M.V.M. is a President Post Doctoral Fellow of the President's Postdoctoral Scholars Program of The Ohio State University. The authors declare that they have no competing interest.

Display items

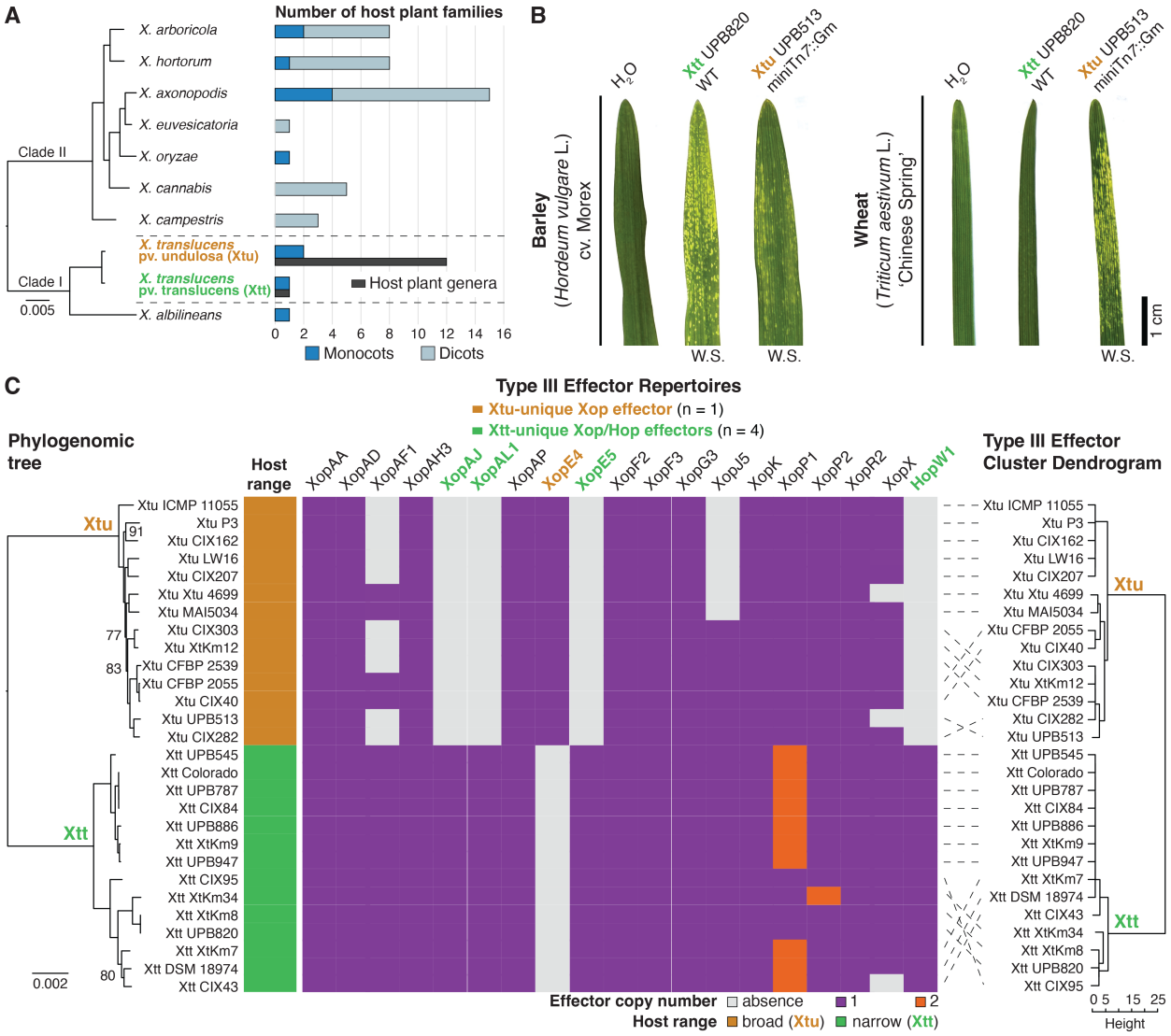

Fig. 1. *X. translucens* pathovars with differential host range breadth encode significantly different effector repertoires. **A.** Phylogenomics and host range of representative *Xanthomonas* spp. The number of plant families that are known hosts (natural or experimentally determined) for each analyzed *Xanthomonas* spp. are shown in the chart to the right side of the panel. The number of plant genera that are known hosts for *X. translucens* pathovars translucens and undulosa is also included in the chart. **B.** Symptom development in barley (*Hordeum vulgare* L. cv. Morex) and wheat (*Triticum aestivum* L. genotype 'Chinese Spring') leaves inoculated (spray) with Xtu and Xtt strains (OD_{600} 0.5) at six days post inoculation. Water soaking symptoms were visualized using a light box and appear as lighter areas in the leaf. Xtt elicited no response in wheat. Scale bar is shown in figure. W.S. – water soaking. **C.** Effector repertoires of *X. translucens* pvs. translucens and undulosa (only non-TAL effectors are presented). A core genome-based tree of 28 *X. translucens* strains is shown to the left side of the panel. Putative Type III secretion system effectors were identified via local Blastx against a database of known *Xanthomonas* effectors. Clustering of strains according to a hierarchical clustering of their

894 encoded repertoires (Type III effector cluster dendrogram) is shown to the right side of the panel.
895 Trees were visualized via FigTree, and mid-point rooted. Branches with bootstrap values below
896 98% are indicated in each tree. Xtt - *X. translucens* pv. translucens; Xtu - *X. translucens* pv.
897 undulosa.
898

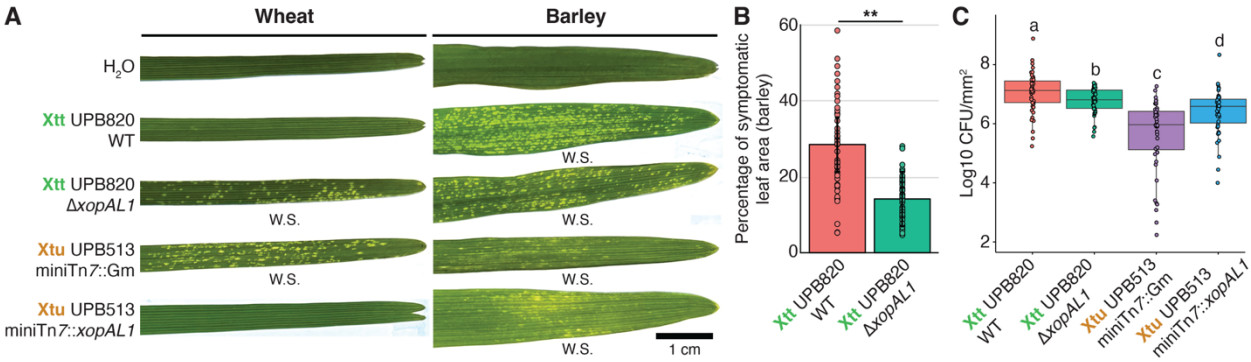

Fig. 2. Deletion of the T3E gene *xopAL1* allows for host jump of Xtt from barley to wheat, while decreasing its pathogenic fitness in barley. **A.** Symptom development in barley and wheat leaves inoculated (spray) with Xtu and Xtt strains (wild-type, mutant, and insertion strains; OD_{600} 0.5) at six days post inoculation. Water soaking symptoms were visualized using a light box and appear as lighter areas in the leaf. Scale bar is shown in figure. **B.** Percentage of symptomatic leaf area of inoculated barley leaves (spray) with Xtt WT and Xtt Δ*xopAL1* shown in panel A. Original data of percentage of symptomatic leaf area (treatments; y-axis) was submitted to a transformation that combines the arcsine and square root functions. The Shapiro-Wilk test (W) was then applied to the transformed data, and it supported the assumption of normal distribution (W = 0.975; *P* value = 0.0671). ** indicates significant difference as determined by Student's *t*-test ($P<0.001$; n = two independent replicates with 23 to 24 biological replicates each). **C.** Xtt and Xtu (wild-type, mutant, and insertion strains) populations in barley leaves inoculated via spray (OD_{600} 0.5) at 144 hours post inoculation. Different letters indicate significant difference as determined by Wilcoxon rank-sum test ($P<0.05$; n = two independent replicates with 23 to 24 biological replicates, each with three internal replicates). Wheat – *Triticum aestivum* L. genotype 'Chinese Spring'; Barley – *Hordeum vulgare* L. cv. Morex; Xtt - *X. translucens* pv. translucens; Xtu - *X. translucens* pv. undulosa; W.S. – water soaking.

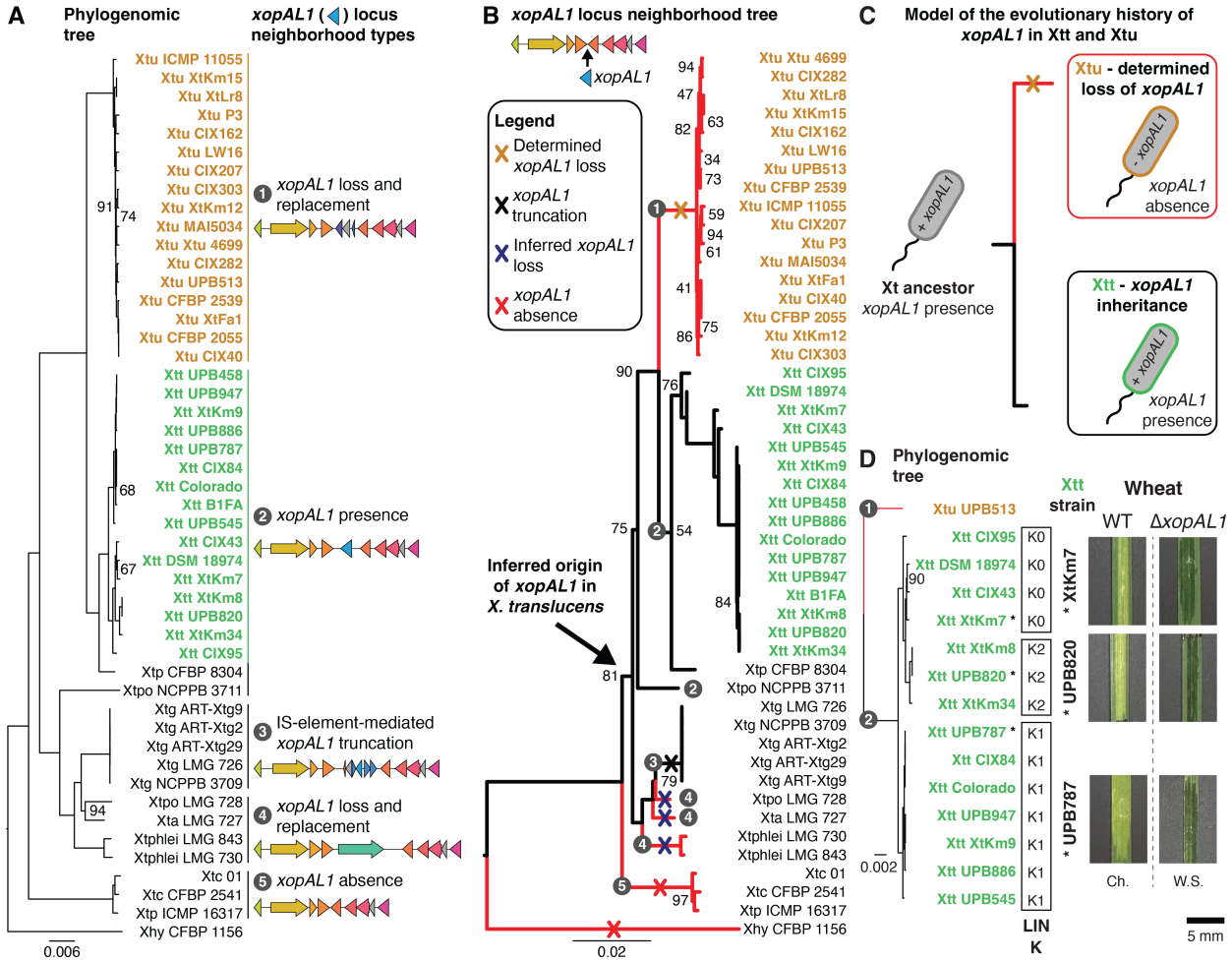

Fig. 3. Loss of *xopAL1* promoted host jump of *X. translucens* pv. undulosa to wheat. **A.** Core genome-based tree of *X. translucens* strains and their *xopAL1* locus neighborhood types. A complete list of genes composing each neighborhood is shown in Fig. S9. **B.** Tree of the concatenated sequences of the genes flanking *xopAL1* in *X. translucens*. The *xopAL1* locus neighborhood types are indicated in each branch. Red-colored branches indicate subgroups that do not encode *xopAL1*, with determined and inferred loss or absence being shown. *X. hyacinthi* strain CFBP 1156 was included as an outgroup to root the trees in panels A and B. **C.** Model of the evolutionary history of *xopAL1* in Xtt and Xtu. **D.** Deletion of *xopAL1* promotes host jump of all Xtt genomic subgroups. A core genome-based tree including the K0, K1 and K2 genomic subgroups of Xtt is shown. Symptom development in wheat (*Triticum aestivum* L. genotype 'Chinese Spring') leaves inoculated (syringe infiltration) with representative Xtt strains (OD_{600} = 0.1) belonging to the three K genomic subgroups and their respective *xopAL1* mutants at three days post inoculation is shown to the right side of the panel. Scale bar is shown in figure. Trees were visualized via Figtree. Branches with bootstrap values below 98% are indicated in each tree. Ch. – chlorosis; W.S. – water soaking. *X. translucens* pathovars: Xtc – pv. cerealis; Xtp – pv. pistaciae; Xtg – pv. graminis; Xtpo – pv. poae; Xta – pv. arrhenateri; Xtphlei – pv. phleipratensis; Xtu – pv. undulosa; Xtt – pv. translucens; Xhy – *X. hyacinthi*.

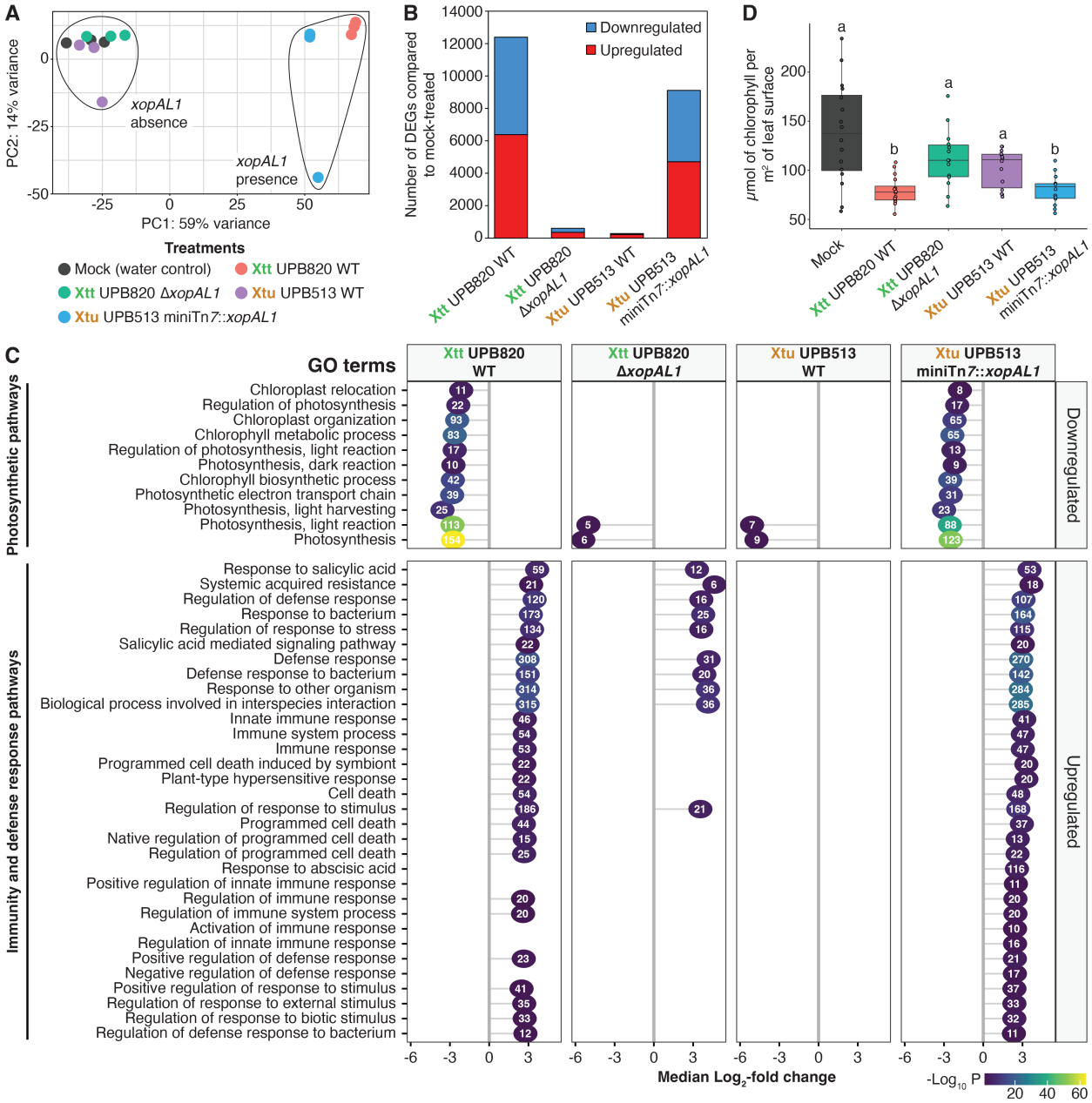

Fig. 4. XopAL1 mediates global transcriptional changes in inoculated wheat plants, leading to a chlorotic non-host response. **A.** Principal component analysis (PCA) of the normalized RNAseq data transcripts per million of wheat leaf tissue infected with different *X. translucens* strains and mock (treatments). Ellipses are arbitrarily drawn to indicate clustering of treatment based on *xopAL1* presence and absence. **B.** Number of significantly differentially expressed genes (DEGs; downregulated and upregulated) in wheat from each bacterial treatment compared to mock. **C.** A subset of Gene Ontology (GO) terms significantly enriched in wheat from bacterial treatments versus mock comparisons. The number of genes that fall into a GO term from each comparison are indicated within each dot. *P* values are indicated by dot color (color scale is shown in figure). Upregulated and downregulated GO terms are indicated in the plot. **D.** Chlorophyll concentration measurement in wheat leaves (*Triticum aestivum* L. genotype 'Chinese Spring') inoculated with Xtt and Xtu strains (wild-type, mutant, and insertion strains) via leaf syringe infiltration (OD_{600}

950 0.1) at three days post inoculation. Different letters indicate significant difference as determined
951 by Wilcoxon rank-sum test ($P<0.05$; n = two independent replicates with 6 to 9 biological
952 replicates, each with three internal replicates). Xtt - *X. translucens* pv. translucens; Xtu - *X.*
953 *translucens* pv. undulosa.
954

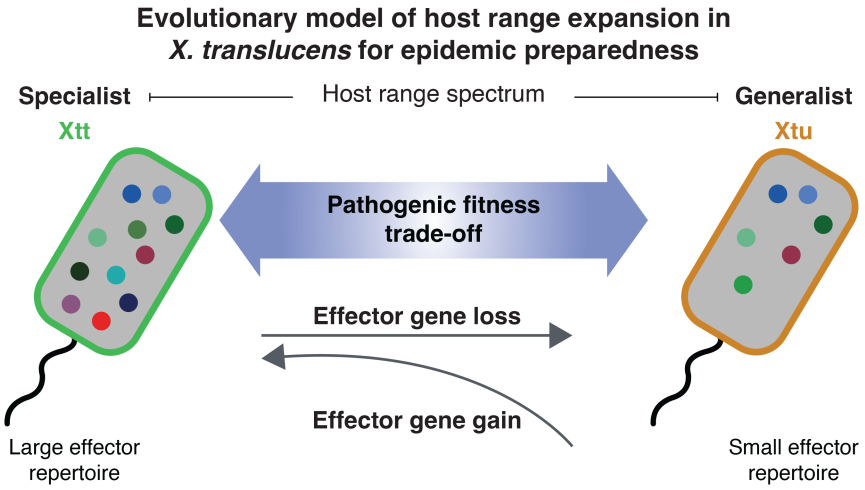

Fig. 5. Proposed evolutionary model of host range expansion in *Xanthomonas translucens* based on effector gene loss and gain. Taken together, phenotypic and phylogenetic analyses support a model where loss of a single Type III secretion system effector gene, *xopAL1*, allowed for host range expansion to wheat by the generalist Xtu, while gain of *xopAJ* in the specialist Xtt restricted even more its host range breadth. Our model also implies that Xtt strains have an inherent risk for host jump via individual losses of *xopAL1* and *xopAJ*, which has profound effects for epidemic preparedness and management practices. Circles with different colors in figure represent different effector repertoires encoded by Xtt and Xtu. Xtt - *X. translucens* pv. translucens; Xtu - *X. translucens* pv. undulosa.